Standish et al., 2019. *Rapid Communications in Mass Spectrometry* **33**, 959–968.

Cite as: Standish, C.D., Chalk, T.B., Babila, T.L., Milton, J.A., Palmer, M.R. and Foster, G,L., 2019. The effect of matrix interferences on in situ boron isotope analysis by laser ablation MC-ICP-MS. *Rapid Communications in Mass Spectrometry* **33**, 959–968.

Doi: 10.1002/rcm.8432

The effect of matrix interferences on *in situ* boron isotope analysis by laser ablation MC-ICP-MS

Christopher D. Standish*, Thomas B. Chalk, Tali L. Babila, J. Andy Milton, Martin R. Palmer & Gavin L. Foster.

School of Ocean and Earth Science, University of Southampton Waterfront Campus, National Oceanography Centre Southampton, European Way, Southampton SO14 3ZH, UK

*corresponding author: C.D.Standish@soton.ac.uk

Abstract

Rationale: Boron isotope analysis of marine carbonates by laser ablation multi-collector inductively coupled plasma mass spectrometry (LA-MC-ICP-MS) offers the potential for rapid sample throughput, and the means to examine micron scale variations in the $\delta^{11}B$ signatures of fossil skeletons and shells/tests of marine organisms. Existing studies demonstrate an acceptable level of reproducibility is achievable, but also typically show a level of accuracy outside the limits required by most applications. Here we investigate matrix interference effects as a cause of inaccuracy and imprecision.

Methods: Analyses were performed on a standard format Thermo Scientific Neptune Plus MC-ICP mass spectrometer coupled to a New Wave Research 193nm ArF laser ablation system. The effects of matrix interference on $\delta^{11}B$ analysis were investigated through analyses of a set of reference materials with differing B/Ca ratios. Three approaches to correct for matrix-induced effects were trialled: 1) use of matrix-matched standards, 2) utilising the relationship between $\delta^{11}B$ inaccuracy and $^{11}B/^{43}Ca$, $^{11}B/^{40}ArCa^{4+}$ or $^{11}B/Ca_{interference}$ from three reference materials with known $\delta^{11}B$ values and varying B/Ca ratios, and 3) direct characterisation of the (sloping) interference itself.

Results: Matrix interference from scattered Ca ions on ^{10}B can impede both the accuracy and reproducibility of $\delta^{11}B$ analysis by LA-MC-ICP-MS. Based on analyses of two in-house reference materials, deep sea coral PS69/318-1 and inorganic calcite UWC-1, we find approach 2, following the $^{11}B/Ca_{interference}$ relationship, gives the best mean accuracies (within 0.4‰ of solution values) and external reproducibilities (± 0.5‰ 2 SD for PS69/318-1). This approach has been applied to analyses of an annual growth cycle of a *Siderastrea siderea* coral and eight *Cibicidoides wuellerstorfi* benthic foraminifera. Both coral and foraminifera data match solution MC-ICP-MS analyses within reported uncertainties.

Conclusions: LA-MC-ICP-MS can produce accurate and precise $\delta^{11}B$ data to a 0.5‰ (2σ) level on <0.3 ng B after correction for Ca interference effects.

Key Words: Boron isotopes; laser ablation; MC-ICP-MS; coral; foraminifera.

1 Introduction

Boron isotope analysis has become a key geochemical tool in the Earth and Planetary sciences.[1] For example, it is employed as a palaeo-pH proxy for seawater in studies concerned with ocean acidification[2,3] and to reconstruct past variations in atmospheric CO_2,[4–7] as a tracer for fluid-rock interactions and mixing processes in the ocean-crust-mantle system,[8,9] and to investigate the timing of condensation and accretion in cosmochemistry.[10,11] This broad utility stems from there being two stable isotopes, ^{10}B and ^{11}B, with a relatively large mass difference leading to large natural isotope variations ($\delta^{11}B$ values of -100‰ to +60‰[12]).

The ratio of $^{11}B/^{10}B$ is typically expressed in delta notation ($\delta^{11}B$) relative to NIST SRM951 as parts per mille (thousand). A range of analytical techniques are available to characterise the $\delta^{11}B$ signature of geological materials, with thermal ionisation mass spectrometry (TIMS) and solution multi-collector inductively coupled plasma mass spectrometry (MC-ICP-MS) achieving the highest precision (<0.3‰).[13] Both techniques involve the analysis of bulk samples which first undergo chemical purification (sample sizes are of the range of 1–1000 ng and 2–50 ng, respectively). These analytical procedures are both time consuming and limited in their ability to characterise potential small-scale isotopic heterogeneities present in the samples, which are of great interest for some applications (e.g. seasonal variability of pH in tropical corals).

Laser ablation (LA)-MC-ICP-MS permits *in situ* analyses of solid samples to investigate small-scale isotopic heterogeneities on a 10–100 μm scale. Further advantages include removing the necessity for sample digestion and purification procedures, thus enabling a greater throughput of samples and reduction of processing blank.[14] LA-MC-ICP-MS $\delta^{11}B$ analyses with external reproducibilities of ± <1‰ (at 2 SD) have been reported for glasses,[15,16] high-B minerals such as tourmaline,[17,18] and high-B steel.[19] External reproducibility of carbonate analyses are typically poorer, between ± 1–1.7‰ (2 SD),[20–22] although Sadekov et al.[23] recently showed external reproducibilities of ± 0.5‰ or better are possible, and Lloyd et al.[22] achieved ± 0.3‰ (2 SD) when reporting the means of ≥10 analyses. Demonstrating accuracy for LA-MC-ICP-MS, however, has proved more challenging, with some studies reporting $\delta^{11}B$ values offset by up to 17‰.[23–26]

LA-MC-ICP-MS analysis is particularly susceptible to matrix-induced effects, which can impede accuracy by altering the instrumental mass fractionation and/or introducing isobaric interferences,[14] as well as laser induced fractionation at the site of ablation.[27] Míková et al.[25] reported a matrix induced bias of up to 2.5‰ when analysing tourmaline, whereas other studies of tourmalines reported matrix dependencies of <1‰.[17,18] Likewise, matrix effects have been reported for carbonates by some studies,[23,24,26] with Sadekov et al.[23] proposing an interference from scattered Ca, C, and O ions, but not by others.[20–22] Both the cause and significance of matrix effects on LA-MC-ICP-MS $\delta^{11}B$ analyses therefore remain unclear.

Sample-standard bracketing routines are typically used to correct for machine induced isotopic fractionation. Most studies employ NIST glasses SRM610 or SRM612,[20,24,26] whilst others have investigated the applicability of in-house, matrix matched, standards.[22,23,25] This approach may mitigate the effects of matrix induced biases, but remains to be fully tested. In this study we examine the influence of Ca-related interference on the accuracy and precision of $\delta^{11}B$ analysis by LA-MC-ICP-MS, and present several methodologies that achieve precise and accurate $\delta^{11}B$ values for a range of carbonates using NIST SRM610 to correct for machine induced isotopic fractionation.

2 Materials and Methods

2.1 Solution MC-ICP-MS

Carbonate reference materials and samples

Solution ICP-MS analysis was performed at the University of Southampton and follow established procedures.[28,29] Coral and calcite reference materials and samples were micro-drilled using a 500 µm drill-bit. Foraminifera were ultrasonicated in 18.2 MΩ cm (ultrapure) water three times then cleaned following standard procedures including an oxidative and final weak acid leach stage.[30] Samples were dissolved in ~0.15 M HNO_3, and separated into two fractions: ~90% for isotopic analysis and ~10% for elemental analysis. Boron was isolated from the carbonate matrix of the isotopic fraction by ion-exchange chromatography using 20 µl Teflon columns filled with Amberlite IRA743 resin. Boron isotope analysis was performed on a Thermo Scientific Neptune MC-ICP mass spectrometer (Thermo Fisher Scientific, Waltham, MA, USA) , with mass bias corrected by sample-standard bracketing with NIST SRM951. Solution concentrations ranged from 5–50 ppb B. Typical 2σ uncertainty is ± 0.2‰ based on a relationship between ^{11}B intensity reproducibility of JCp-1.[31] The trace element fractions were diluted and measured on a Thermo Scientific Element 2-XR ICP mass spectrometer,[32] with B/Ca ratios precise and accurate to ± 4% (2σ).

Silicate reference materials

Preparation of silicate samples follow procedures adapted from Wei et al.[33] Samples were dissolved in 24 M HF and mannitol. Boron was then isolated from the silicate matrix by ion-exchange chromatography using columns containing 80 µl of Bio-Rad AG MP-1M anion exchange resin (Bio-Rad Laboratories, Hercules, CA, USA). Boron isotope analysis was performed on a Thermo Scientific Neptune MC-ICP mass spectrometer following the method described in Foster[28] but with a 0.3 M HF and 0.5 M HNO_3 wash solution to reduce memory effects. Mass bias was corrected by sample-standard bracketing with NIST SRM951, and samples were run at ~200 ppb concentrations. Typical in-run 2σ precisions are <0.4‰.

2.2 Standards and Reference Materials

All standards and reference materials analysed in this study, selected to cover a range of B concentrations and B/Ca ratios, are listed in Table 1. JCp-1 (*Porites sp.* coral[34]) and JCt-1 (biogenic aragonite *Tridacna gigas*[35]) are well-characterised, with collated values from interlaboratory comparison studies preferred here: Gutjahr et al.[36] for $\delta^{11}B$ values and Hathorne et al.[37] for B/Ca ratios. Synthetic carbonate reference material MACS-3,[38] calcite UWC-1 from the Valentine Wollastonite Mine in the Adirondacks, USA,[39] cold water calcitic scleraxonian octocoral PS69/318-1,[40,41]

as well as the widely available silicate standard NIST SRM610, were all characterised using the relevant solution MC-ICP-MS methodologies outlined in 2.1. Foster et al.[29] powdered both UWC-1 and PS69/318-1 prior to $\delta^{11}B$ analysis by solution MC-ICP-MS, naming them IC_B and IC_C respectively, whilst Kasemann et al.[40] previously analysed both standards using a variety of analytical techniques (SIMS, solution MC-ICP-MS and TIMS). Here we used new fragments of each standard.

The fragment of PS69/318-1 analysed has a lower $\delta^{11}B$ value than those published by Kasemann et al.[40] and Foster et al.[29]; 13.83 ± 0.29‰ (2 SE) compared to 16.07 ± 1.33‰ (2 SD) and 15.55 ± 0.23‰ (2σ) respectively. We interpret this difference to reflect large-scale heterogeneity within the coral specimen from which fragments were obtained, but there was no indication of isotopic heterogeneity within the fragment analysed in this study. UWC-1 also demonstrates isotopic heterogeneity, with the individual crystals (A to C) analysed characterised by $\delta^{11}B$ values of 7.28 ± 0.50‰ (2 SE) to 8.15 ± 0.28‰ (2 SE), but these are consistent with previously published values from Foster et al.[29] and Kasemann et al.[40]; 8.35 ± 0.45‰ (2σ) and 8.08 ± 1.16‰ (2 SD) respectively. $\delta^{11}B$ variation for these materials on the cm scale means caution should be exercised with respect to using the values cited here for other fragments of the same reference materials. Solution analyses of NIST SRM610 gave a mean $\delta^{11}B$ value of -0.26 ± 0.13‰ (2 SD), matching previous measurements by solution MC-ICP-MS of -0.26 ± 0.28‰ (2 SD).[15]

Table 1. Solution MC-ICP-MS ($\delta^{11}B$) and ICP-MS (B/Ca in µmol/mol) analysis of B isotope reference materials.

ID	Details	$\delta^{11}B$	2 SE	B/Ca	2 SE	B (ppm)	Reference
NIST SRM610	Glass (NIST)	-0.26	0.23	-	-	-	This study
		-0.28	0.27	-	-	-	This study
		-0.17	0.24	-	-	-	This study
		-0.32	0.44	-	-	-	This study
		Mean = -0.26 ± 0.13 (2 SD)		-	-	-	This study
MACS-3	Synthetic carbonate pellet (USGS)	-0.51	0.38	55	2.2	5.92	This study
		-0.62	0.34	56	2.2	6.06	This study
		-0.57	0.33	57	2.3	6.11	This study
		Mean = -0.57 ± 0.11 (2 SD)		Mean = 56 ± 2 (2 SD)		Mean = 6.03	This study
JCt-1	Pellet of aragonite, *Tridacna gigas* (JGS)	16.3	0.55	191	9 (SD)	20.65	[36,37]
JCp-1	Pellet of *Porites sp*. coral (JGS)	24.3	0.42	460	23 (SD)	49.73	[36,37]
PS69/318-1	Cold water calcitic scleraxonian octocoral	13.83	0.29	198	7.9	21.40	This study
UWC-1	Inorganic calcite rhomb, Valentine Wollastonite Mine	8.15	0.28	148	5.9	16.00	This study
		7.89	0.24	145	5.8	15.67	This study
		7.28	0.50	133	5.3	14.38	This study
		Mean = 7.77 ± 0.89 (2 SD)		Mean = 142 ± 16 (2 SD)		Mean = 15.35	This study

2.3 Laser Ablation MC-ICP-MS

Methodology

Laser ablation B isotope analysis was performed at the University of Southampton using a standard format Thermo Scientific Neptune Plus MC-ICP mass spectrometer equipped with nine Faraday Cup detectors and a central ion counter (with a

Retarding Potential Quadrupole lens), coupled to a New Wave Research 193nm ArF laser ablation system with TwoVol2 ablation cell (Elemental Scientific Lasers, Bozeman, MT, USA). Prior to analysis, samples and reference materials were prepared following a variety of methods. NIST glasses and fragments of PS69/318-1 and UWC-1 were mounted in epoxy resin and polished. Uncleaned, powdered, JCp-1 and JCt-1 were pressed into pellet form using a manual hydraulic press (mass of 10 t over a period of 30 minutes). A ~5 mm thick core slice of a *Siderastrea siderea* coral was polished and mounted onto a glass slide. Foraminifera were cleaned individually as whole tests to limit test breakage and maintain chamber integrity by ultrasonicating three times in ultrapure water to remove surficial clays, then gently placed on double sided tape with the umbilicus side facing upward.

LA-MC-ICP-MS tuning protocols were designed to achieve maximum sensitivity to enable analysis of a full range of sample materials (B/Ca ratios of 56 to 460 µmol/mol). Operating conditions are outlined in Table S1; typical operating parameters for the laser ablation system were: beam diameter of 100–150 µm, repetition rate of 12 Hz, power density of ~6 J cm^{-2}, line or raster ablation mode tracking at 10 µm s. Prior to data collection, the samples were ablated using the above laser parameters or, for the powdered pellets and foraminifera tests, with reduced power (50%) and repetition rate (5 Hz) and increased speed (100 µm/s), to remove any surface contamination present.

Analyses of reference materials integrate 25 cycles, foraminifers 30 cycles, and coral samples 50 cycles, all peak hopping between selected cup configurations detailed in Table S2. Configuration 1 collects ^{10}B and ^{11}B, whilst peak hopping to configuration 2 allows the collection of $^{11}B/^{40}ArCa^{4+}$ (where $^{40}ArCa^{4+}$ is the mass peak consisting of quadrupley charged mass 40 ions of both Ar and/or Ca) and peak hopping to configuration 3 allows collection of $^{11}B/^{43}Ca$. Faraday Cup detectors were used in all instances, with 10^{12} Ω resistors installed on all relevant cups except for the centre cup where a 10^{11} Ω resistor was used due to the large ^{43}Ca beam intensity. An on-peak gas blank was analysed before and after ablation (both 40 seconds duration), with 24 seconds allowed for sample wash-out prior to the latter. Idle times of 2 seconds were required when protocols included configuration 2, and idle times of 3 seconds were required when protocols included configuration 3.

For all ratios, on-peak blank and instrumental mass bias corrections were applied offline. Dynamic blank corrections were applied cycle by cycle assuming a linear relationship between the preceding and succeeding blank measurements. Instrumental mass bias was corrected by sample-standard bracketing with glass reference material NIST SRM610 and using the isotope composition presented in Table 1 and published by le Roux et al.[15] Data were screened with those cycles falling outside of 3 SD of the mean removed. Typically, two analyses of NIST SRM610 would bracket an analysis of each of the three reference pellets (JCp-1, JCt-1, MACS-3) and no more than ~12 minutes ablation of other reference materials or samples. Based on a 25 cycle peak hopping analyses between configuration 1 (B isotopes) and configuration 2 ($^{40}ArCa^{4+}$), and typical operating conditions, a single analysis consumes between ~50 pg (MACS-3) and ~300 pg (JCp-1) of B. Taking only the time spent on configuration 1 collecting ^{10}B and ^{11}B data, this equates to between ~15 pg and ~80 pg B for the $^{11}B/^{10}B$ ratio itself.

In order to fully investigate the nature of background interferences, mass scans using Faraday Cup detectors were run from *m*/*z* 9.667 to 11.167 over 800 steps. Scans of reference materials were collected for 1 hour with integration times of 0.524 s, whilst a scan of the gas blank was collected for ~18 hours with integration times of 1 s. Mass scans of the gas blank using the ion counter were collected over two discreet mass ranges to avoid the $^{40}ArCa^{4+}$ peak: *m*/*z* 9.667 to 9.984 (300 steps, ~2 hour duration) and *m*/*z* 9.987 to 11.167 (800 steps, ~9 hour duration), both using 1 s integration times.

Accuracy & Precision

Typical accuracy and precision of laser ablation $\delta^{11}B$ analysis was determined through repeat analyses of the pellet reference materials JCp-1, JCt-1 and MACS-3 over a 5 month period (Figure 1). Internal precisions (2 SE) vary with the B concentration, with mean internal precisions ranging from ± 1.33‰ for MACS-3 (6 ppm B) to ± 0.55‰ for JCp-1 (50 ppm B). Mean $\delta^{11}B$ values (± 2 SD) were 19.11 ± 2.50‰ for JCp-1, 7.55 ± 2.84‰ for JCt-1, and -15.77 ± 8.85‰ for MACS-3 (n = 45 for all), equating to mean inaccuracies ($\Delta\delta^{11}B$, defined as $\delta^{11}B_{solution}$ - $\delta^{11}B_{laser}$) of 5.19‰, 8.75‰, and 15.20‰ respectively. Notably, the differences between reference materials are larger between sessions than within sessions. Likely causes of the reported external reproducibility and inaccuracy are explored below.

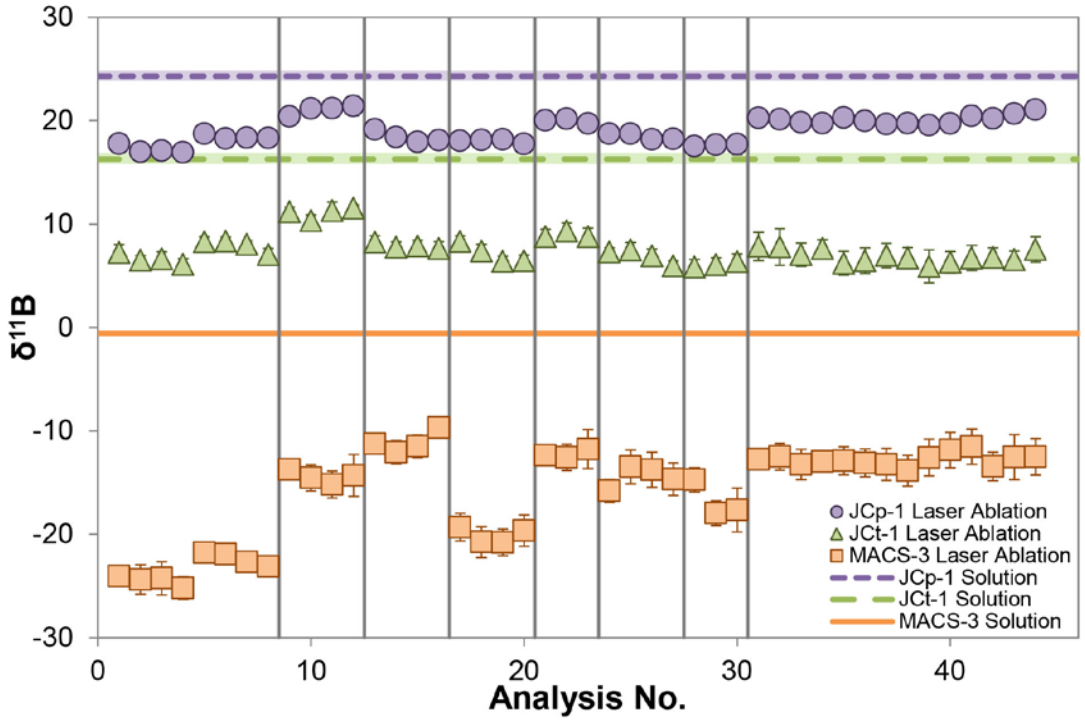

Figure 1. LA-MC-ICP-MS $\delta^{11}B$ analyses of reference materials JCp-1, JCt-1 and MACS-3 over a 5 month period. Vertical grey lines separate analytical sessions. Error bars on the laser ablation analyses are ± 2 SE of the mean of 25 integration cycles. Uncertainties on solution values are ± 2 SD.

3 Matrix induced effects

Blank corrected $^{11}B/^{10}B$ ratios are independent of laser spot size, repetition rate, and ^{43}Ca intensity changes (Figure S1), suggesting that both laser-induced fractionation and matrix loading are not the primary cause of the $\delta^{11}B$ inaccuracy evident in Figure 1. To explore the potential influence of isobaric and other forms of interferences,

Figure 2 shows a series of mass scans from *m*/*z* 9.7 to 11.1 – i.e. across the B isotope mass range – of a typical gas blank and analyses of both NIST SRM610 and carbonate JCt-1. The gas blank is shown using both Faraday Cup and ion counter detectors, whilst NIST SRM610 and JCt-1 are shown using Faraday Cup detection only. Although not fully resolved, the $^{40}ArCa^{4+}$ is resolved sufficiently to suggest that tailing across the ^{10}B peak cannot explain the level of inaccuracy reported here. However, the faraday cup scans show a clear, elevated, background signal of ≥0.1 mV across the entire mass window similar to that demonstrated by Sadekov et al.[23] This background signal is further elevated in the JCt-1 mass scan relative to those of the NIST SRM610 and gas blank at *m*/*z* lower than ~11.0. This additional background elevation is likely to be matrix related, and critically, because it is of a lower intensity in both the gas blank and NIST SRM610 it will not be corrected for in either the on-peak blank or the mass bias corrections. Therefore, in agreement with Sadekov et al.[23], we propose this as the most likely cause of the reported inaccuracy and associated external reproducibility shown in Figure 1.

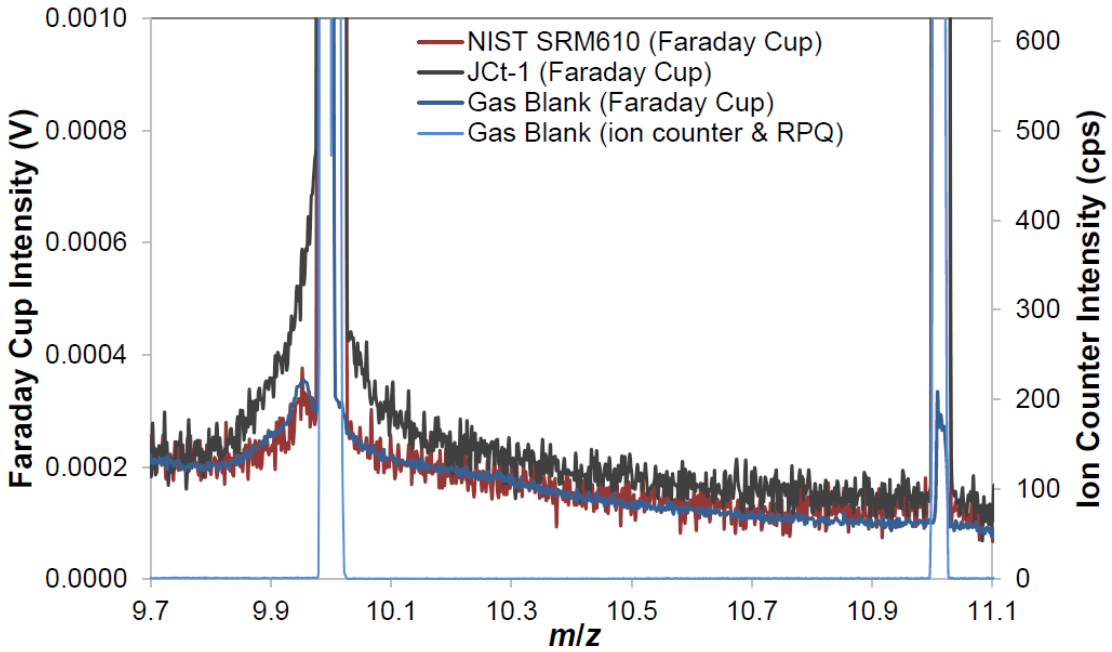

Figure 2. JCt-1, NIST SRM610, and gas blank mass scans across the $^{40}ArCa^{4+}$, ^{10}B and ^{11}B peak range. Gas blank mass scans are shown using both Faraday Cup (dark blue) and ion counter (light blue) detectors, whilst the JCt-1 (grey) and NIST SRM610 (red) mass scans are shown using a Faraday Cup detector only.

With this elevated background being largest around *m*/*z* of 10 and minimal at *m*/*z* of 11, it follows that variable interference would lead to inaccurately low $\delta^{11}B$ values – i.e., as illustrated in Figure 1. The calculated scale of such an interference on ^{10}B for JCt-1, necessary to cause the observed inaccuracy, is of the order of 0.2–0.4 mV (depending on analytical session). Based on the mass scans illustrated Figure 2, the difference in the background at ^{10}B between JCt-1 and NIST SRM610 is of the same order of magnitude, consistent with the hypothesis that this elevated background is the cause of the recorded inaccuracy.

It is evident from Figure 2 that the elevated background signal has an irregular shape, suggesting it is not a well-defined mass. Furthermore, although it is relatively diffuse, it apparently peaks to the low mass side of the $^{40}ArCa^{4+}$ where *m*/*z* is 9.95, and

therefore is not a peak relating simply to quadrupley charged mass 40 ions which have a *m*/*z* of ~9.99. However, given that Ca is the key matrix component in JCt-1 (~39 wt%), it is likely related to Ca ions, and indeed a log-law relationship exists between $\Delta\delta^{11}B$ and B/Ca (Figure 3). The same relationship is also present between $\Delta\delta^{11}B$ and both $^{11}B/10.59$ and $^{11}B/^{40}ArCa^{4+}$, and this will be the case for $^{11}B/m$ where *m* is any mass where an elevated background signal is present. This relationship suggests that the raised background, across the entire mass range scanned, is predominantly Ca related. Similar relationships between B/Ca and accuracy of $\delta^{11}B$ measurements are evident in tourmalines as measured by Míková et al.[25]; Figure S2.

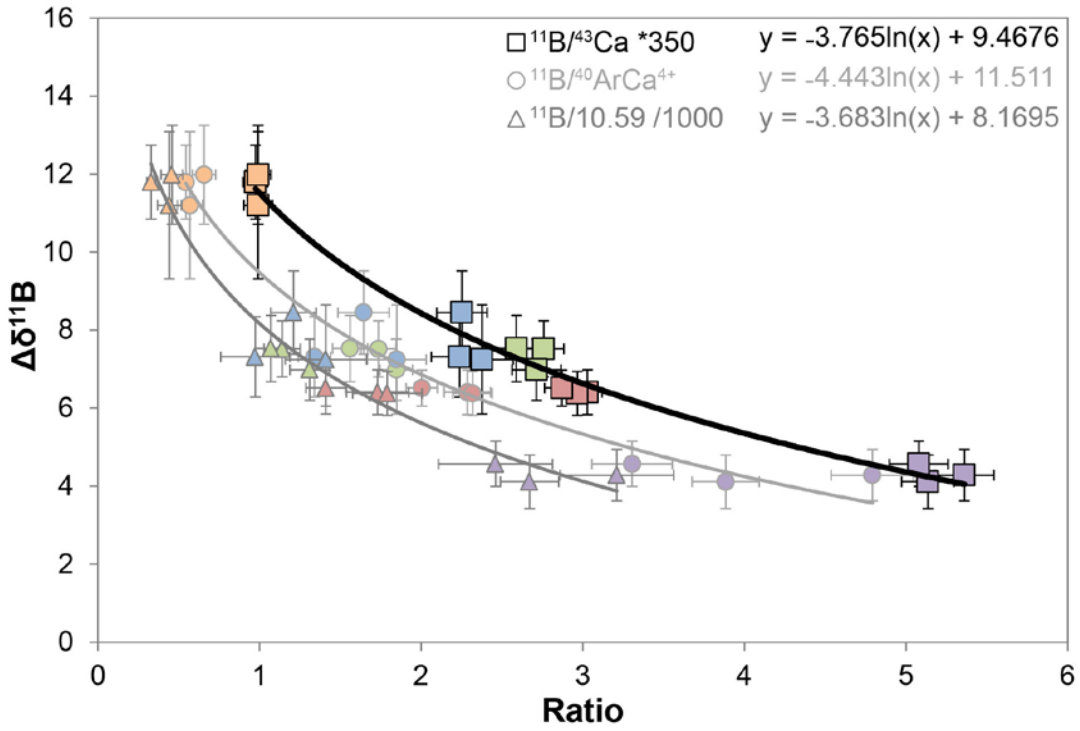

Figure 3. $\Delta\delta^{11}B$ versus $^{11}B/^{43}Ca$, $^{11}B/10.59$ and $^{11}B/^{40}ArCa^{4+}$of reference materials MACS-3 (orange), UWC-1 (blue), JCt-1 (green), PS69/318-1 (red) and JCp-1 (purple). Error bars are ± 2 SE of the mean of 25 integration cycles.

An ion counter gas blank mass scan is also shown in Figure 2, and it is evident that the elevated background recorded by the Faraday Cup is not present. An important difference between the detection modes is the presence of a Retarding Potential Quadrupole lens (RPQ) when using ion counter detection, which filters ions whose energy levels have been disturbed. The RPQ thus eliminates scattered ions, e.g. those reflected off the flight tube, to give reduced backgrounds and less peak tailing. The elevated background documented when using Faraday Cup detectors can therefore be linked to scattering of Ca ions. Bailey[42] reached similar conclusions after identifying a raised background when employing LA-MC-ICP-MS for Sr isotope analysis.

Tuning for: 1) plasma conditions that minimise ionisation of Ca relative to B (e.g. by varying the RF power), 2) minimised ion scattering, and 3) improved abundance sensitivity, is therefore likely to improve accuracy and precision of $\delta^{11}B$ analysis by laser ablation MC-ICP-MS. This may account for the different degrees of matrix effects observed in previous LA-MC-ICP-MS studies.[20,22] In addition, ion scatter may

behave differently in different models of MC-ICP-MS. Protocols that tune out this interference are, however, only likely to be successful when analysing samples with higher B/Ca ratios such as corals, as such protocols typically lead to a loss in sensitivity. Furthermore, because the elevated background around ^{10}B is likely to be present to some extent in all studies that employ laser ablation MC-ICP-MS without the use of an energy filtering device to determine $\delta^{11}B$ in carbonates or Ca-bearing minerals, it is important to demonstrate accuracy across a range of B/Ca ratios before applying the technique to unknown samples.

4 Correcting for matrix induced bias

4.1 Matrix-matched standards

The relationship between $\Delta\delta^{11}B$ and B/Ca suggests that matrix-matched standards may enable accurate and precise measurement of $\delta^{11}B$, and indeed Lloyd et al.[22] have demonstrated success with such a protocol. In this study, the two reference materials with the most similar B/Ca ratios are JCt-1 and PS69/318-1 (191 µmol/mol and 198 µmol/mol respectively). The mean $\delta^{11}B$ value (± 2 SD) of PS69/318-1 when using NIST SRM610 as the bracketing standard is 6.08 ± 1.87‰ ($\Delta\delta^{11}B$ of 7.75). The mean $\delta^{11}B$ value (± 2 SD) of PS69/318-1 when using JCt-1 as the bracketing standard is 15.07 ± 1.12‰ ($\Delta\delta^{11}B$ of -1.24); Figure 4 and Table 2. While using JCt-1 therefore clearly improved $\delta^{11}B$ accuracy and reproducibility, there still remains an offset. This may be because the sample and standard used here are not similar enough, or because of the differing physical properties of the two materials – JCt-1 is a pressed pellet and therefore ablates differently to PS69/318-1 with a higher Ca yield. Either way, this suggests that, at least with the set-up used in the present study, standards will need to be very well matched or inaccuracies will still exist.

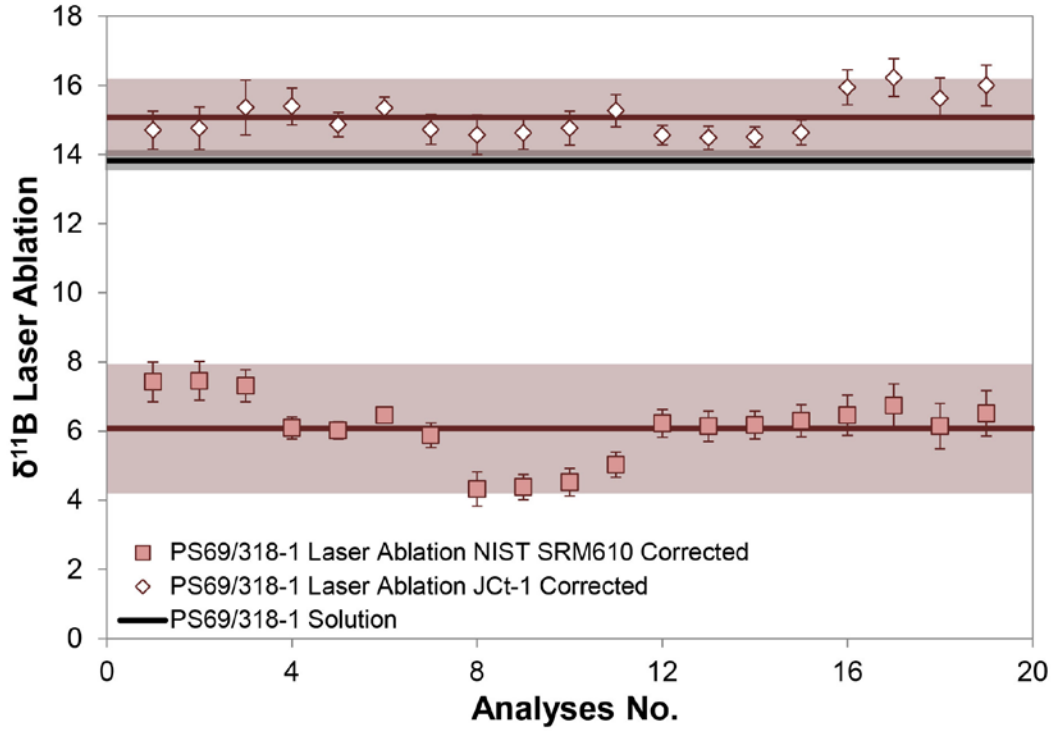

Figure 4. Laser ablation MC-ICP-MS analyses of coral PS69/318-1 (Ca = 40 wt%) when using NIST SRM610 (poorly matrix matched; Ca = 8.1 wt%) and JCt-1 (improved matrix matching; Ca = 39 wt%) as bracketing standards. Error bars are ± 2 SE of the mean of 25 integration cycles. Mean values (± 2 SD) are also shown.

Table 2. Summary of matrix-corrected $\delta^{11}B$ values of reference materials following the different approaches.

Reference Material		1) ~Matrix-matched	2) Relationship between $\Delta\delta^{11}B$ and B/Ca			3) Slope of Ca interference
			$^{11}B/^{40}ArCa^{4+}$	$^{11}B/10.59$	$^{11}B/^{43}Ca$	
JCp-1	Mean ± 2 SD					23.65 ± 1.13
	Mean $\Delta\delta^{11}B$					0.65
	n					7
JCt-1	Mean ± 2 SD					16.98 ± 0.55
	Mean $\Delta\delta^{11}B$					-0.68
	n					7
PS69/318-1	Mean ± 2 SD	15.07 ± 1.12	14.12 ± 0.73	14.23 ± 0.47	13.9 ± 0.79	13.92 ± 0.45
	Mean $\Delta\delta^{11}B$	-1.24	-0.29	-0.40	-0.07	-0.09
	n	19	15	15	7	8
UWC-1	Mean ± 2 SD		7.27 ± 1.47	7.39 ± 1.63	8.49 ± 2.45	8.43 ± 1.36
	Mean $\Delta\delta^{11}B$		0.50	0.38	-0.72	-0.66
	n		7	7	7	4

4.2 The relationship between $\Delta\delta^{11}B$ and B/Ca

A matrix correction can also be applied to the data using the relationship between $\Delta\delta^{11}B$ and B/Ca (Figure 3). By analysing a series of reference materials with known $\delta^{11}B$ values and varying B/Ca ratios, this relationship can be defined throughout any analytical session and used to matrix-correct analyses of 'unknowns'. If the reference materials cover the full range of possible B/Ca ratios found in typical sample material – as is the case here for marine carbonates – then such a method has the scope to give accurate and precise $\delta^{11}B$ values for a range of different geological materials, removing the need for closely matrix-matched standards. Figure 3 shows that there is a well-defined log-relationship between $\Delta\delta^{11}B$ and $^{11}B/^{43}Ca$, but use of this relationship requires a peak hopping protocol with a large mass jump and magnet settling times of ≥3 seconds. This reduces the efficiency of the analysis with respect to time and ultimately the spatial resolution of the analytical protocol; following this method a single cycle of 10.4 s only spends 2.197 s integrating $^{11}B/^{10}B$ data. This means that ~80% of each analysis is not spent collecting B isotope data, and the potential spatial resolution is reduced.

Because the Ca interference occurs across the entire B mass range, the same relationship also exists between $\Delta\delta^{11}B$ and any mass where this interference is present, for example $^{11}B/10.59$ (i.e. direct characterisation of the Ca interference at an *m/z* of 10.59, so $^{11}B/Ca_{interference}$) or $^{11}B/^{40}ArCa^{4+}$ (Figure 3). These two ratios offer alternative methods for matrix-correcting the data. The former has the advantage that data can be collected statically, allowing analyses at the highest spatial resolution possible in the minimum time, but the 10.59 signal intensity is low – on the order of ~1 mV – limiting precision of the analysis. In contrast the $^{40}ArCa^{4+}$ peak is larger (on the order of 80–90 mV), but requires a peak hopping approach, albeit with a smaller mass jump than when peak hopping to ^{43}Ca.

Accuracy and external reproducibility for all methods are compared by analysis of the inorganic calcite UWC-1 and the cold water calcitic scleraxonian octocoral PS69/318-1 (Table 2, Figure 5). Whilst all data obtained from the three approaches agree to within 0.3‰ for PS69/318-1 and 1.1‰ for UWC-1, and the majority of the

matrix corrected $\delta^{11}B$ data are within analytical uncertainty of the solution values (Figure 5), the best combined accuracy and external reproducibility is achieved using the $^{11}B/10.59$ (i.e. $^{11}B/Ca_{interference}$) approach; mean $\delta^{11}B$ values of both PS69/318-1 and UWC-1 are within 0.4‰ of solution values. Furthermore, this approach allows static collection of data and therefore ultimately analyses at the greatest spatial resolution, though it should be noted that here the proportion of time spent collecting $^{11}B/^{10}B$ data is the same for each method presented. It is also important to note that the lower reproducibility of the UWC-1 analyses is similar to the level of $\delta^{11}B$ variability documented between ablated chips by solution analyses (Table 1) suggesting that elevated uncertainty for this sample largely reflects small-scale $\delta^{11}B$ heterogeneity.

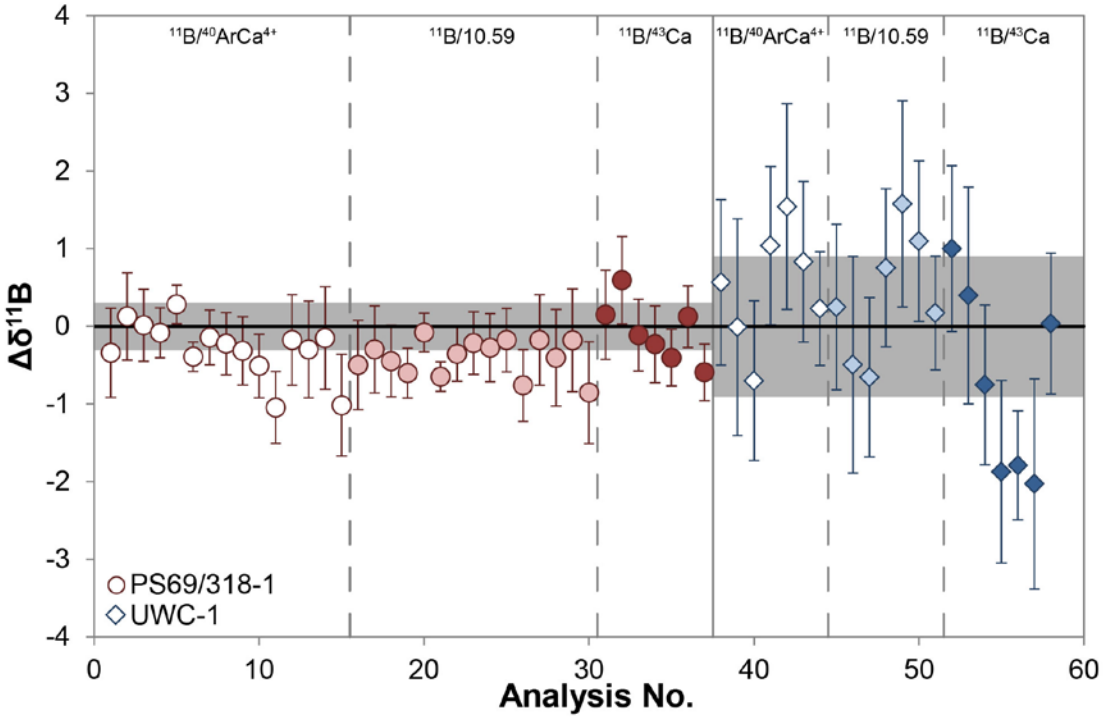

Figure 5. Laser ablation versus solution MC-ICP-MS $\delta^{11}B$ analyses of UWC-1 and PS69/318-1 reference materials prior to, and after, matrix correction. Matrix corrections use the log-relationships between $\Delta\delta^{11}B$ and either $^{11}B/^{40}ArCa^{4+}$, $^{11}B/^{43}Ca$, or $^{11}B/10.59$ of reference materials MACS-3, JCt-1 and JCp-1. Error bars for LA analyses are ± 2 SE of the mean of 25 integration cycles.

4.3 The slope of the Ca interference

The Ca interference increases towards lower masses peaking at *m*/*z* ~9.95 (Figure 2). In an attempt to correct the interference directly, Faraday Cup detectors L1 and L2 were both equipped with 10^{12} Ω resistors, and were positioned as close to the ^{10}B peak as possible (at *m*/*z* 10.18 and 10.10 respectively; configuration 1 in Table S2) to characterise the steepest part of the interference slope on the high mass side of ^{10}B. Using a linear relationship between $^{11}B/Interference_{mass}$ versus $Interference_{mass}$ (i.e. the mass chosen to measure the interference; inset Figure 6), the interference at ^{10}B was calculated and subtracted from the ^{10}B measured intensity after on-peak gas blank subtraction and prior to mass bias correction with bracketing analyses of NIST SRM610 (Table 2, Figure 6). All the analyses lie within 1.30‰ of the solution values, but only half are within 0.50‰, whilst internal precisions are typically ± 0.7–0.9‰ (2 SE). Although this method does not require additional standards (other than NIST

SRM610), the accuracy, internal precision and external reproducibility are not as good as the approaches that use the relationship between $\Delta\delta^{11}B$ and $^{11}B/^{43}Ca$, $^{11}B/10.59$ or $^{11}B/^{40}ArCa^{4+}$ outlined in 4.2 (Figure 5). This result may arise from the use of only a 2-point regression to determine the irregular interference magnitude at ^{10}B, and may be improved if a third Faraday Cup detector can be placed on the interference slope (although the inclusion of the centre cup in this regression does not improve the correction). In addition, because the Ca interference being measured has a low signal intensity, use of 10^{13} Ω resistors may also improve the correction.

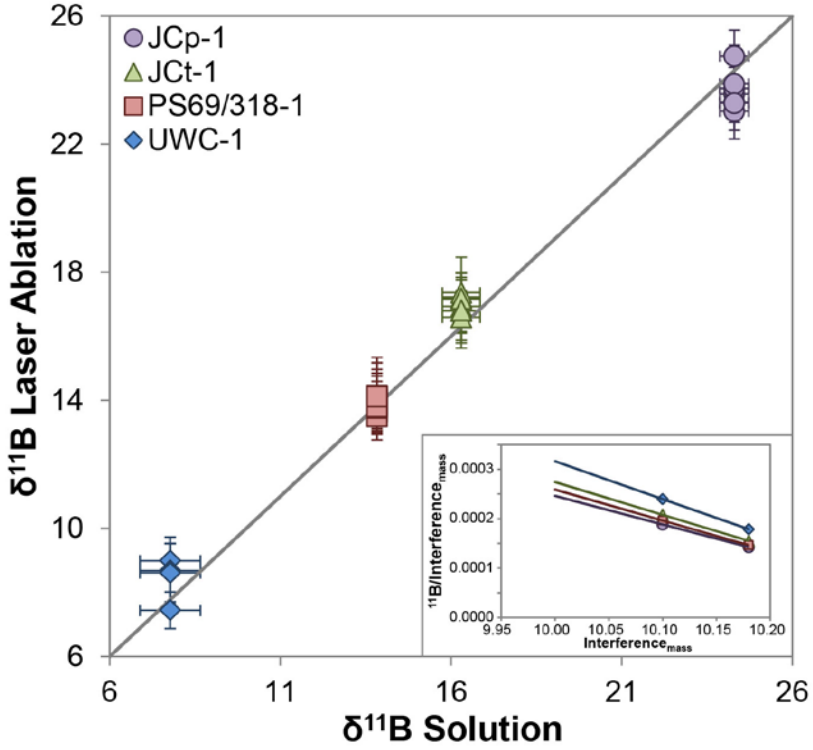

Figure 6. Laser ablation versus solution MC-ICP-MS $\delta^{11}B$ analyses of JCp-1, JCt-1, PS69/318-1 and UWC-1 following matrix correction based on the slope of the Ca interference measured at *m*/*z* 10.18 and *m*/*z* 10.10. Error bars are ± 2 SE of the mean of 25 integration cycles. Inset: examples of the relationship between $^{11}B/Interference_{mass}$ and $Interference_{mass}$ used for matrix correction.

5 Application to geological samples

5.1 *Siderastrea siderea*

The utility of the $^{11}B/10.59$ method can be further demonstrated by analysis of geological samples. First, an annual cycle of a *Siderastrea siderea* specimen from the Southern Belize portion of the Mesoamerican Barrier Reef System was analysed by both solution and laser ablation MC-ICP-MS techniques; two laser line-tracks were ablated and compared to two micro-drill (solution) tracks sampled from adjacent theca walls of this coral (Figure 7). For the isotopically homogenous JCp-1 and PS69/318-1, 2 SE on the mean $\delta^{11}B$ values of 8 consecutive cycles in line mode are typically ± 0.4–0.5‰, therefore 2σ internal uncertainties of ± 0.5‰ are considered appropriate for the 8 cycle means of the sample laser transects also. Mean $\delta^{11}B$ values (± 2 SE) for the laser transects are 22.74 ± 0.59‰ and 22.80 ± 0.50‰. These are within analytical uncertainty of mean $\delta^{11}B$ values obtained from solution analyses of the two micro-drill transects (22.32 ± 0.68‰ and 23.04 ± 0.85‰

respectively). Furthermore, the laser ablation method also resolves the seasonal $\delta^{11}B$ cycles revealed using the solution techniques. Differences between the shape of the cycles are perhaps expected given the spatially variable $\delta^{11}B$ signature revealed by the laser ablation analyses coupled with the lower spatial resolution of the solution analyses (140 μm laser beam diameter versus 500 μm drill-bit for solution analysis), and slight differences between the exact skeletal element analysed. It should also be noted that, without the need for intensive chemical cleaning and separation in the laboratory, laser ablation precludes the requirement to include a procedural blank which can be both important and difficult to fully characterise on small sample sizes; it can account for ~0.5% of the total boron analysed.

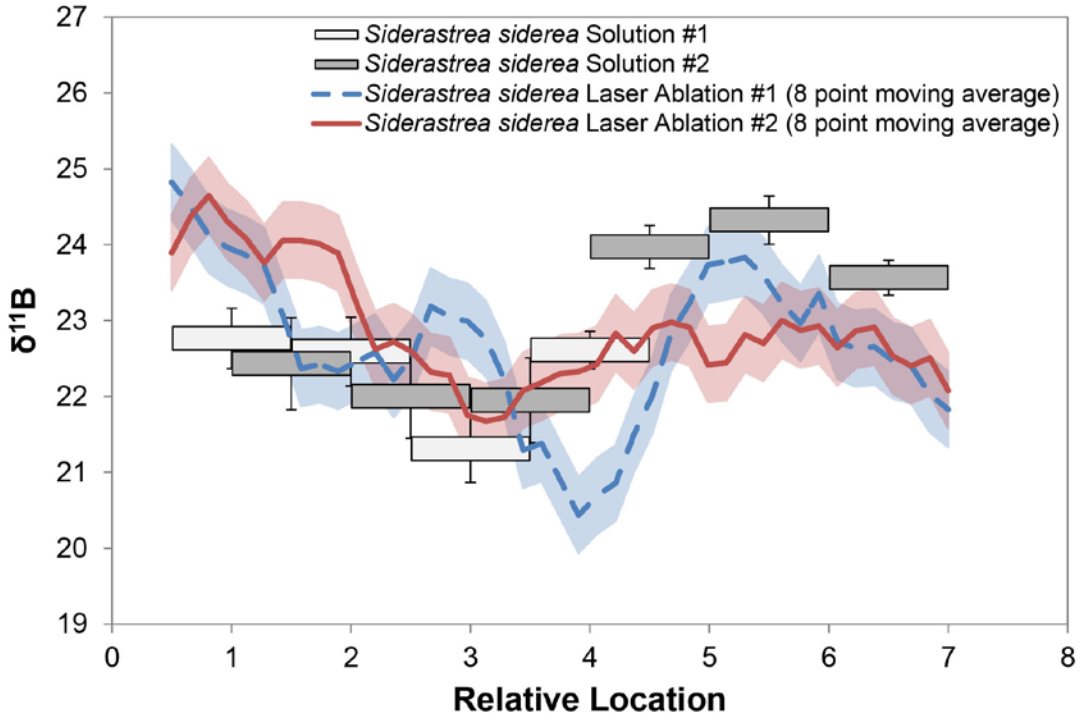

Figure 7. Comparison of laser ablation and solution MC-ICP-MS $\delta^{11}B$ analyses of a *Siderastrea siderea* specimen from the Mesoamerican Barrier Reef System. Laser tracks are an 8-point moving average with uncertainties of ± 0.5‰ (2σ).

5.2 *Cibicidoides wuellerstorfi*

A population of 8 benthic foraminifera tests (*Cibicidoides wuellerstorfi*) from the same sample depth of ODP Site 999 was also analysed by both the $^{11}B/10.59$ LA-MC-ICP-MS approach and solution methods (Figure 8). Note that by cleaning and dissolving what remained of the ablated tests (see methods) we can be sure of the true $\delta^{11}B$ value of the mean of the analysed foraminifera. Solution analysis of all foraminiferal tests post-ablation gave a $\delta^{11}B$ value of 16.30 ± 0.22‰ (2 SE). Individual tests analysed by LA-MC-ICP-MS ranged from 15.85 ± 0.75‰ (2 SE) to 16.58 ± 0.78‰ (2 SE), with a mean 16.10 ± 0.48‰ (2 SD). This result indicates that there is limited resolvable variability in the $\delta^{11}B$ values between individual tests for this species, and further demonstrates the accuracy and potential of the laser ablation methodology presented here.

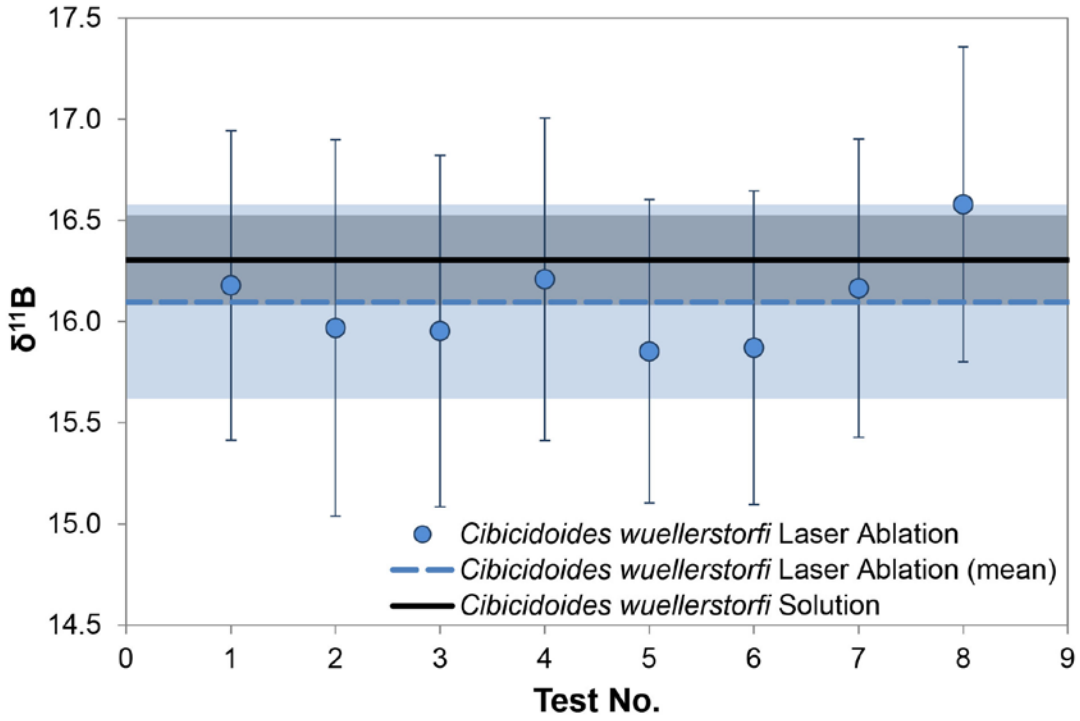

Figure 8. Comparison of laser ablation and solution MC-ICP-MS $\delta^{11}B$ analyses of *Cibicidoides wuellerstorfi* tests from ODP Site 999. Error bars are ± 2 SE of the mean of 25 integration cycles. Uncertainty on the solution analysis is ± 2 SE, and on the mean laser ablation analysis is ± 2 SD.

6 Conclusions

Determining the boron isotopic composition of carbonates using laser ablation has many advantages, including: ease of analysis, high sensitivity (<0.3 ng vs ~20 ng of B required), and high spatial resolution. However, numerous authors have reported issues with both accuracy and precision. In agreement with Sadekov et al.[23] we have identified a matrix interference from scattered Ca ions on ^{10}B, and have trialled three alternative correction approaches applicable to analysis by standard format MC-ICP-MS: 1) the use of matrix-matched standards, 2) using the relationship between inaccuracy and $^{11}B/^{43}Ca$, $^{11}B/^{40}ArCa^{4+}$ or $^{11}B/Ca_{interference}$ for three reference materials with known $\delta^{11}B$ values and varying B/Ca ratios, and 3) direct characterisation of the (sloping) interference. Approach 2, using the inaccuracy versus $^{11}B/Ca_{interference}$ relationship, gives the best external reproducibilities based on repeat analyses of two reference materials: deep sea coral fragment PS69/318-1 (± 0.5‰; 21.4 ppm B) and inorganic calcite UWC-1 (±1.6‰; 15.4 ppm B), and mean accuracies of within 0.4‰ of the solution values. This approach has been further demonstrated through the analyses of an annual growth cycle of a *Siderastrea siderea* coral from the Southern Belize portion of the Mesoamerican Barrier Reef System, and a set of eight *Cibicidoides wuellerstorfi* foraminifera from ODP Site 999. Both match solution MC-ICP-MS analysis within the reported uncertainties but at a fraction of the sample size.

Acknowledgements

Dan Doran and Matthew Beverley-Smith of the Rock Preparation and Thin-Sectioning Laboratories, University of Southampton, are thanked for preparation of the reference materials and coral section prior to analysis by LA-MC-ICP-MS.

Matthew Cooper and Agnes Michalik for acknowledged for their analytical help and Clive Trueman for making the MicroMill available for use. Funding was provided by the Leverhulme Trust.

References

1. Marschall HR, Foster GL. Boron Isotopes in the Earth and Planetary Sciences—A Short History and Introduction. In: Marchall H, Foster G, ed. *Boron Isotopes: The Fifth Element*. Advances in Isotope Geochemistry. Cham, Switzerland: Springer; 2018:1–11.
2. McCulloch M, Trotter J, Montagna P, et al. Resilience of cold-water scleractinian corals to ocean acidification: boron isotopic systematics of pH and saturation state up-regulation. *Geochim Cosmochim Acta.* 2012;87:21–34. doi.org/10.1016/j.gca.2012.03.027.
3. Fowell SE, Foster GL, Ries JB, et al. Historical trends in pH and carbonate biogeochemistry on the Belize Mesoamerican Barrier Reef System. *Geophys Res Lett.* 2018;45:3228–3237. doi.org/10.1002/2017GL076496.
4. Anagnostou E, John EH, Edgar KM, et al. Changing atmospheric CO_2 concentration was the primary driver of early Cenozoic climate. *Nature.* 2016;533: 380–384. doi.org/10.1038/nature17423.
5. Foster GL, Rae JWB. Reconstructing Ocean pH with Boron Isotopes in Foraminifera. *Annu Rev Earth Planet Sci.* 2016;44:207–37. doi.org/10.1146/annurev-earth-060115-012226.
6. Chalk TB, Hain MP, Foster GL, et al. Causes of ice age intensification across the Mid-Pleistocene Transition. *Proc Natl Acad Sci USA.* 2017;114(50): 13114–13119. doi.org/10.1073/pnas.1702143114.
7. Sosdian SM, Greenop R, Hain MP, Foster GL, Pearson PN, Lear CH. Constraining the evolution of Neogene ocean carbonate chemistry using the boron isotope pH proxy. *Earth Planet Sci Lett.* 2018;498:362–376. doi.org/10.1016/j.epsl.2018.06.017.
8. De Hoog JCM, Savov IP. Boron Isotopes as a Tracer of Subduction Zone Processes. In: Marchall H, Foster G, ed. *Boron Isotopes: The Fifth Element*. Advances in Isotope Geochemistry. Cham, Switzerland: Springer; 2018:217–247.
9. Marschall HR. Boron Isotopes in the Ocean Floor Realm and the Mantle. In: Marchall H, Foster G, ed. *Boron Isotopes: The Fifth Element*. Advances in Isotope Geochemistry. Cham, Switzerland: Springer; 2018:189–215.
10. Hoppe P, Goswami JN, Krähenbühl U, Marti K. Boron in chondrules. *Meteorit Planet Sci.* 2001;36:1331–1343. doi.org/10.1111/j.1945-5100.2001.tb01828.x.
11. Liu M-C, Chaussidon M. The Cosmochemistry of Boron Isotopes. In: Marchall H, Foster G, ed. *Boron Isotopes: The Fifth Element*. Advances in Isotope Geochemistry. Cham, Switzerland: Springer; 2018:273–289.
12. Foster GL, Lecuyer C, Marschall HR. Boron Stable Isotopes. In: White WM, ed. *Encyclopeda of Geochemistry*. Encyclopedia of Earth Sciences Series. Berlin: Springer; 2016:1–6.
13. Foster GL, Marschall HR, Palmer MR. Boron Isotope Analysis of Geological Materials. In: Marchall H, Foster G, ed. *Boron Isotopes: The Fifth Element*. Advances in Isotope Geochemistry. Cham, Switzerland: Springer; 2018:13–31.
14. Pearson NJ, Griffin WL, O'Reilly SY. Mass fractionation correction in laser ablation multiple-collector ICP-MS: implications for overlap corrections and precise and accurate in situ isotope ratio measurement. In: Sylvester P, ed.

Laser ablation-ICP-MS in the Earth sciences: current practices and outstanding issues. Mineralogical Association of Canada; 2008:93–116.
15. le Roux PJ, Shirley SB, Benton L, Hauri EH, Mock TD. In situ, multiple-multiplier, laser ablation ICP-MS measurement of boron isotopic composition (δ11B) at the nanogram level. *Chem Geol.* 2004;203:123–138. doi.org/10.1016/j.chemgeo.2003.09.006.
16. Devulder V, Gerdes A, Vanhaecke F, Degryse P. Validation of the determination of the B isotopic composition in Roman glasses with laser ablation multi-collector inductively coupled plasma-mass spectrometry. *Spectrochim Acta Part B At Spectrosc.* 2015;105:116–120. doi.org/10.1016/j.sab.2014.08.038.
17. Hou KJ, Li YH, Xiao YK, Liu F, Tian YR. In situ boron isotope measurements of natural geological materials by LA-MC-ICP-MS. *Chin Sci Bull.* 2010;55: 3305–3311. doi.org/10.1007/s11434-010-4064-9.
18. Ribeiro da Costa I, Mourao C, Recio C, et al. Tourmaline occurrences within the Penamacor-Monsanto granitic pluton and host-rocks (Central Portugal): genetic implications of crystal-chemical and isotopic features. *Contrib Mineral. Petrol.* 2014;167:993–1016. doi.org/10.1007/s00410-014-0993-7.
19. Kurta C, Dorta L, Mittermayr F, et al. Rapid screening of boron isotope ratios in nuclear shielding materials by LAICPMS – a comparison of two different instrumental setups. *J Anal Atom Spectrom.* 2014;29:185–192. doi.org/10.1039/C3JA50194A.
20. Fietzke J, Heinemann A, Taubner I, Böhm F, Erez J, Eisenhauer A. Boron isotope ratio determination in carbonates via LA-MC-ICP-MS using soda-lime glass standards as reference material. *J Anal Atom Spectrom.* 2010;25:1953–1957. doi.org/10.1039/C0JA00036A.
21. Kaczmarek K, Horn I, Nehrke G, Bijma J. Simultaneous determination of $\delta^{11}B$ and B/Ca ratio in marine biogenic carbonates at nanogram level. *Chem Geol.* 2014;392:32–42. doi.org/10.1016/j.chemgeo.2014.11.011.
22. Lloyd NS, Sadekov AY, Misra S. Application of 10^{13} ohm Faraday cup current amplifiers for boron isotopic analyses by solution mode and laser ablation multicollector inductively coupled plasma mass spectrometry. *Rapid Commun Mass Spectrom.* 2017;32: 9–18. doi.org/10.1002/rcm.8009.
23. Sadekov AY, Lloyd NS, Misra S, Trotter J, D'Olivo J, McCulloch M. Accurate and precise microscale measurements of boron isotope ratios in calcium carbonates using Laser Ablation Multicollector-ICPMS. *J Anal Atom Spectrom.* 2019. doi.org/10.1039/C8JA00444G.
24. Gerdes A. Boron isotopes analyses of carbonates, phosphates and silicates by laser ablation MC-ICP-MS: the influence of sample matrix. In: *American Geophysical Union Fall Meeting 2013. Abstract V51F-03, San Francisco: AGU, 9–13 December 2013*. 2013. http://adsabs.harvard.edu/abs/2013AGUFM.V51F..03G.
25. Míková J, Košler J, Wiedenbeck M. Matrix effects during laser ablation MC ICP-MS analysis of boron isotopes in tourmaline. *J Anal Atom Spectrom.* 2014;29:903–914. doi.org/10.1039/C3JA50241D.
26. Thil F, Blamart D, Assailly C, et al. Development of laser ablation multi-collector inductively coupled plasma mass spectrometry for boron isotopic measurements in marine biocarbonates: new improvements and application to a modern *Porites* coral. *Rapid Commun Mass Spectrom.* 2016;30: 359–371. doi.org/10.1002/rcm.7448.

27. Jackson SE, Günther D. The nature and sources of laser induced isotopic fractionation in laser ablation-multicollector-inductively coupled plasma-mass spectrometry. *J Anal Atom Spectrom.* 2003;18:205–212. doi.org/10.1039/B209620J.
28. Foster GL. Seawater pH, pCO2 and CO3 2- variations in the Caribbean Sea over the last 130 kyr: A boron isotope and B/Ca study of planktic foraminifera. *Earth Planet Sci Lett.* 2008;271:254–266. doi.org/10.1016/j.epsl.2008.04.015.
29. Foster GL, Hönisch B, Paris G, et al. Interlaboratory comparison of boron isotope analyses of boric acid, seawater and marine $CaCO_3$ by MC-ICPMS and NTIMS. *Chem Geol.* 2013;358:1–14. doi.org/10.1016/j.chemgeo.2013.08.027.
30. Barker S, Greaves M, Elderfield H. A study of cleaning procedures used for foraminiferal Mg/Ca paleothermometry. *Geochem Geophy Geosystems.* 2003;4: 8407. doi.org/10.1029/2003GC000559.
31. Rae JWB, Foster GL, Schmidt DN, Elliott T. Boron isotopes and B/Ca in benthic foraminifera: Proxies for the deep ocean carbonate system. *Earth Planet Sci. Lett.* 2011;302:403–413. doi.org/10.1016/j.epsl.2010.12.034.
32. Henehan MJ, Foster GL, Rae JWB, et al. Evaluating the utility of B/Ca ratios in planktic foraminifera as a proxy for the carbonate system: A case study of Globigerinoides ruber. *Geochem Geophy Geosystems.* 2015;16:1052–1069. doi.org/10.1002/2014GC005514.
33. Wei G, Wei J, Liu Y, et al. Measurement on high-precision boron isotope of silicate materials by a single column purification method and MC-ICP-MS: *J Anal Atom Spectrom.* 2013;28:606–612. doi.org/10.1039/C3JA30333K.
34. Okai T, Suzuk, A, Kawahata H, Terashima S, Imai N. Preparation of a new Geological Survey of Japan geochemical reference material: Coral JCp-1, *Geostand Newslett.* 2002;26: 95–99. doi.org/10.1111/j.1751-908X.2002.tb00627.x.
35. Inoue M, Nohara M, Okai T, Suzuki A, Kawahata H. Concentrations of trace elements in carbonate reference materials coral JCp-1 and giant clam JCt-1 by inductively coupled plasma-mass spectrometry. *Geostand Geoanal Res.* 2004;28(3):411–416. doi.org/10.1111/j.1751-908X.2004.tb00759.x.
36. Gutjahr M, Bordier L, Douville E, et al. Boron Isotope Intercomparison Project (BIIP): development of a new carbonate standard for stable isotopic analyses. *Geophysical Research Abstracts* 2014;16:EGU2014-5028-2011. http://adsabs.harvard.edu/abs/2014EGUGA..16.5028G.
37. Hathorne EC, Gagnon A, Felis T, et al. Interlaboratory study for coral Sr/Ca and other element/Ca ratio measurements. *Geochem Geophy Geosystems.* 2013;14(9):3730–3750. doi.org/10.1002/ggge.20230.
38. Chen L, Liu Y, Hu Z, et al. Accurate determinations of fifty-four major and trace elements in carbonate by LA-ICP-MS using normalization strategy of bulk components as 100%. *Chem Geol.* 2011;284: 283–295. doi.org/10.1016/j.chemgeo.2011.03.007.
39. Gerdes ML, Valley JW. Fluid flow and mass transport at the Valentine wollastonite deposit, Adirondack Mountains, New York State. *J Metamorph Geol.* 1994;12:589–608. doi.org/10.1111/j.1525-1314.1994.tb00045.x.
40. Kasemann SA, Schmidt DN, Bijma J, Foster GL. *In situ* boron isotope analysis in marine carbonates and its application for foraminifera and palaeo-pH. *Chem Geol.* 2009;260:138–147. doi.org/10.1016/j.chemgeo.2008.12.015.
41. Gutjahr M, Vance D, Hoffmann DL, et al. Structural limitations in deriving accurate U-series ages from calcitic cold-water corals contrast with robust coral

radiocarbon and Mg/Ca systematics. *Chem Geol.* 2013;355:69–87. doi.org/10.1016/j.chemgeo.2013.07.002.

42. Bailey TE. Applications of strontium isotope stratigraphy: the potential of laser micro-sampling. 2001. Unpublished PhD thesis, Royal Holloway University of London.